Three-Dimensional Reconstruction of *Macrobdella decora* (Leech) Hemoglobin by Cryoelectron Microscopy

Felix de Haas,* Nicolas Boisset,* Jean-Christophe Taveau,* Olivier Lambert,* Serge N. Vinogradov,‡ and Jean N. Lamy*

*Laboratoire des Protéines Complexes et CNRS URA 1334, Université de Tours, F-37032 Tours Cedex, France, and ‡Wayne State University, Department of Biochemistry, Detroit, Michigan 48201 USA

ABSTRACT   *Macrobdella decora* hemoglobin was observed in vitreous ice by cryoelectron microscopy and subjected to three-dimensional reconstruction by the method of random conical tilt series. The refined volume has a resolution of 40 Å and a D_6 point-group symmetry. Its architecture, with its hexagonal bilayer appearance, resembles those of *Lumbricus terrestris* (oligochaete) and *Eudistylia vancouverii* (polychaete). When the reconstruction volume is viewed along its sixfold axis, the vertices of the upper hexagonal layer are rotated 16° clockwise compared to those of the lower layer. In agreement with the "bracelet" model of Vinogradov et al., a central linker complex is decorated by 12 hollow globular substructures. The linker complex is made up of a central hexagonal toroid linked by 12 c5 connections to two bracelets of c3 connections, which are themselves linked via six c4 connections. The portion of the hollow globular substructure corresponding to the dodecamer of globin chains has a local pseudo threefold symmetry and is composed of three elongated structures visible when the volume is displayed at high threshold. The main difference between *Macrobdella*, *Lumbricus*, and *Eudistylia* hemoglobins is the presence in *Macrobdella* of a central hexagonal toroid instead of a compact flat hexagonal structure.

INTRODUCTION

Multimeric extracellular macromolecular oxygen carriers termed erythrocruorin or chlorocruorin occur in oligochaetes, polychaetes, and leeches. In the electron microscope, they appear as hexagonal bilayer (HBL) structures (Vinogradov et al., 1982; Antonini and Chiancone, 1977; Boekema and Van Heel, 1989; Kapp et al., 1990; Ilan and Haroun, 1993). Despite a large number of biochemical studies, the stoichiometry of the polypeptide chains composing these multimeric proteins is still under investigation.

For *Lumbricus terrestris* hemoglobin (oligochaete) Vinogradov et al. (1986, 1991) have proposed a model based on 144 globin chains arranged in 12 dodecamers decorating a bracelet of 36 heme-deficient linker chains. An alternative model with 192 globin chains and 24 (L1, L2, and L3) linker chains was suggested by Ownby et al. (1993) based on subunit stoichiometry determined by reverse-phase high-performance liquid chromatography. Recently Martin et al. (1996b) determined the molecular weight of the component polypeptide chains by mass spectrometry and proposed a refined model based on 12 dodecamers of globin chains and 36 linker chains (12 L1, 6 L2, 12 L3, and 6 L4). In the case of *Tylorrhincus heterochaetus* hemoglobin (polychaete), Gotoh and Suzuki (1990) and Green et al. (1995) have advanced a model consisting of 12 dodecamers and 36 linker chains. *Eudistylia vancouverii* chlorocruorin

(polychaete) also appears to consist of 12 dodecamers of globin chain and 30 to 40 linker chains (Qabar et al., 1991). The bracelet model, adapted to the hemoglobin of the leech *Macrobdella decora* (achaete) to interpret the sodium dodecyl sulfate/polyacrylamide gel electrophoresis data of Kapp et al. (1990), also led to a model comprising 12 dodecameric units and 30 to 40 linker chains. On the basis of mass spectrometric determinations Weber et al. (1995) found that a model comprising 144 functional globin chains (12 dodecameric units) and 42 linker chains (6 chain C, 24 D, and 12 E) provided the best fit to the 3.5 MDa mass and known physical properties of this hemoglobin.

The bracelet architecture is also supported by three-dimensional (3D) reconstructions at low resolution obtained by cryoelectron microscopy for *Lumbricus terrestris* hemoglobin (Schatz et al., 1995) and *Eudistylia vancouverii* chlorocruorin (de Haas et al., 1995). These 3D volumes are composed of 12 hollow globular substructures (HGSs) associated in a HBL by several substructures presumed to correspond to the linker chains.

The present 3D reconstruction of *Macrobdella* hemoglobin computed from electron microscopic (EM) images of a frozen-hydrated specimen confirms this hypothesis and demonstrates that annelid hemoglobins and chlorocruorins have similar quaternary structures that differ only in minor structural details.

MATERIALS AND METHODS

Sample preparation and cryoelectron microscopy

A sample of *M. decora* hemoglobin (0.1 mg/ml) was prepared as described elsewhere (Weber et al., 1995) by dilution in a 0.1 M Tris-HCl buffer, pH 7.2, 10 mM $CaCl_2$, 10 mM $MgCl_2$. Approximately 5 μl of the solution was applied to a 300-mesh copper grid, coated with a perforated carbon film.

After blotting the excess solution, we quickly plunged the grid into liquid ethane (Dubochet et al., 1988; Adrian et al., 1984; Milligan et al., 1984). Using a Gatan 626 cryotransfer system, we loaded the specimen into a Philips CM12 electron microscope equipped with a Gatan CCD camera and a Gatan 651N anticontaminator maintained at a temperature of $-175°C$ and examined it at an accelerating voltage of 100 kV and a magnification of ×32,514, determined from the diffraction pattern of a catalase crystal (Misell, 1978). Micrographs were recorded with a minimum dose on Kodak SO 163 films and developed in full-strength Kodak D19 developer for 12 min. Each specimen field was recorded twice, with the grid respectively tilted at 45° and 0°, and received an electron dose of 9 $e^-/Å^2$, assessed by the conversion efficiency of the CCD camera. Pairs of micrographs were recorded at defocus values of -2.5 (underfocus) and -2.0 μm for the tilted specimen and the untilted specimen fields, respectively. Because of the tilt angle of 45°, the value of -2.5 μm corresponds to a mean defocus of the tilted specimen micrograph. However, inasmuch as the top and side views are almost completely missing in the tilted specimen images, this procedure did not completely cover the whole angular range. A second series of micrographs taken with the specimen untilted at a defocus of -2.0 μm was added to complement the angular range. Because of the gradient of defocus, the 3D reconstruction volume shown in this article was not subjected to contrast transfer function (CTF) correction.

Image processing

Micrographs were digitized with an Optronix P1000 drum microdensitometer using a square aperture and a scan step of 25 μm corresponding to a pixel size of 0.77 × 0.77 nm in the specimen. The same particles were windowed from the tilted and untilted specimen micrographs on a Silicon Graphics workstation, using an interactive selection program. The tilt angle and direction of the tilt axis were calculated at this step from the particle coordinates (Radermacher, 1988). All selected particles coded as an array of optical densities were windowed, contrast inverted, and normalized so that their noise statistics would match a reference distribution corresponding to a portion of micrograph free of particles and artifacts (Boisset et al., 1993). All programs used for image processing are part of the SPIDER (Frank et al., 1981a) and SIGMA (Taveau and Lamy, 1990; Taveau, 1996) softwares.

The 3D reconstruction was carried out by the method of random conical tilt series (Radermacher et al., 1987a,b), as modified by Penczek et al. (1992, 1994). The complete set of untilted specimen images was first subjected to reference-free two-dimensional (2D) alignment and sorted into homogeneous image classes by correspondence analysis (Van Heel and Frank, 1981) and hierarchical ascendent classification (Van Heel, 1984) using Ward's merging criterion (Ward, 1963; Lebart et al., 1984). Then the tilted specimen images corresponding to the top and side views were subjected to 3D reconstruction, using a χ^2 minimization iterative algorithm

(Penczek et al., 1992). To reach an isotropic resolution, the corresponding primary 3D reconstruction volumes were aligned in a common orientation by the method of direct search in real space (Penczek et al., 1992). Rather than adding the primary volumes, a merged 3D reconstruction was processed from the selected original classes of tilted specimen images after correcting their assigned Eulerian angles. Finally, the merged 3D reconstruction volume was refined with several cycles of 3D projection alignment (Penczek et al., 1994). At this stage, tilted specimen images initially disregarded because of their low frequency occurrence or their atypical overall shapes (intermediate views) were included in the image set from which the final 3D reconstruction volume was computed. For the resolution limit estimation of 2D averages and 3D volumes, two subsets were randomly drawn from the whole image set. The corresponding pairs of 2D averages or 3D volumes were then compared in reciprocal space on increasing radii or spherical shells with the differential phase residual (DPR) (Frank et al., 1981b), using a phase residual threshold of 45° and the Fourier shell correlation (Saxton and Baumeister, 1982) criteria.

Determination of C_6 or D_6 point-group symmetry

To test for the D_6 point-group symmetry of the reconstructed molecule, we followed a method described for cylindrical particles (Lambert et al., 1995). In this method, the C_6-symmetrized volume is first stepwise rotated around its sixfold axis with a 2° increment. At each step, a correlation coefficient between the volume in its original and rotated positions is calculated, producing the reference curve (not shown). As a C_6 point-group symmetry is imposed on the 3D reconstruction volume, the correlation coefficient reaches the maximum value of 1.0 every 60°. To test the possibility of a D_6 point-group symmetry, a similar curve (not shown) is drawn. However, previous to the rotation around the sixfold axis, the volume is 180° rotated around an axis located in the equatorial plane of the molecule and perpendicular to the sixfold axis. The hypothesis of a D_6 point-group symmetry is accepted if the test curve, similar to the reference curve, reaches a correlation coefficient value close to 1.0 every 60°.

Exploration and visualization of the volume

All of the operations of visualization of the reconstructed 3D volumes by surface rendering, slice extraction, and contouring were carried out with the SIGMA software (Taveau, 1996).

RESULTS

Cryoelectron microscopy

A typical pair of untilted and tilted specimen fields of frozen-hydrated *Macrobdella* hemoglobin is shown in Fig.

FIGURE 1 A frozen-hydrated sample of *Macrobdella decora* hemoglobin observed in cryo EM. Views of the same field of the specimen untilted (*A*) and tilted (*B*). Three types of EM views are observed in the untilted frame (*A*). Top views (*white arrows*) have an overall hexagonal shape. Side views (*black arrows*) have a rectangular shape. Intermediate views (*black circles*) correspond to undefined orientations with oval external contours. The corresponding particles are labeled similarly in the tilted frame (*B*), but their appearance is modified by the tilting. The bar corresponds to a distance of 50 nm.
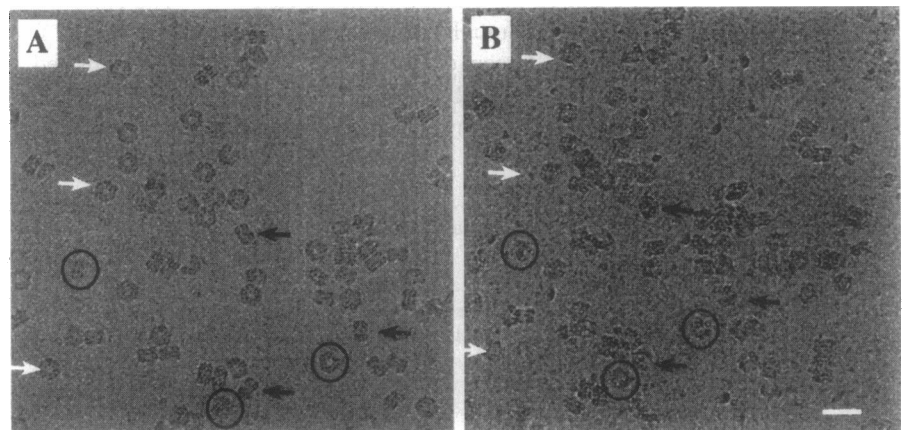
1. In the untilted specimen field (Fig. 1 *A*), the particles appear in two well-defined orientations: top (*white arrows*) and side (*black arrows*) EM views. In the top view, the molecule is observed along its sixfold axis and has a hexagonal overall shape, whereas in the side view it shows a bilayered rectangular pattern. The particles may also produce approximately oval views termed *intermediate* views (*black circles*). In the untilted specimen micrographs the relative occurrence of the top, side, and intermediate EM views were estimated to 58%, 28%, and 14%, respectively. These proportions indicate that the particles are not randomly oriented in the ice layer because of an air-water interface phenomenon or due to a too small thickness of the ice layer.

Image processing and 3-D reconstruction

A series of 955 pairs of tilted and untilted specimen single particle images and a series of 613 untilted specimen images were first interactively selected and windowed. Then, after 2D alignment, the untilted specimen images of the first series were subjected to multivariate statistical analysis and automatic clustering to sort image classes homogeneous with respect to the specific orientations of the particles within the ice layer. Cutting the aggregation dendrogram (Fig. 2) produced by the hierarchical ascendent classification at level 1 produced four main image classes corresponding to top (Fig. 2, *A* and *B*), intermediate (Fig. 2 *C*), and side (Fig. 2 *D*) views. At level 2, 33 homogeneous smaller image classes were obtained. For the top and side views the resolution limit was in the range of 46.6 ± 1.5 Å and 36.7 ± 2.2 Å when estimated by the DPR (with a phase residual threshold of 45°) and Fourier ring correlation method, respectively. Intermediate EM views produced numerous small classes with very low resolution limits.

Fig. 2, *E–K*, shows the average images computed from the untilted specimen images of the seven classes of top and side views selected for 3D reconstruction. Of these seven classes, two corresponding to top views have a sixfold symmetry and look very similar (Fig. 2, *E* and *F*). The other five, corresponding to side views, i.e., to HBL molecules observed perpendicularly to their sixfold axis, have a twofold symmetry and present different distributions of their densities (Fig. 2, *G–K*).

The tilted specimen images corresponding to the seven classes of Fig. 2, *E–K*, were independently subjected to 3D reconstruction. Then the seven resulting primary volumes were aligned in a common orientation by 3D alignment in real space, and a merged 3D reconstruction volume was computed from the seven corresponding classes of tilted specimen images. Because the whole molecule has an obvious sixfold symmetry, the merged volume was computed with an enforced C_6 point-group symmetry. Nevertheless, the architecture of the resulting merged reconstruction volume suggested that besides a sixfold symmetry the molecule may have six twofold axes, i.e., a D_6 point-group symmetry.
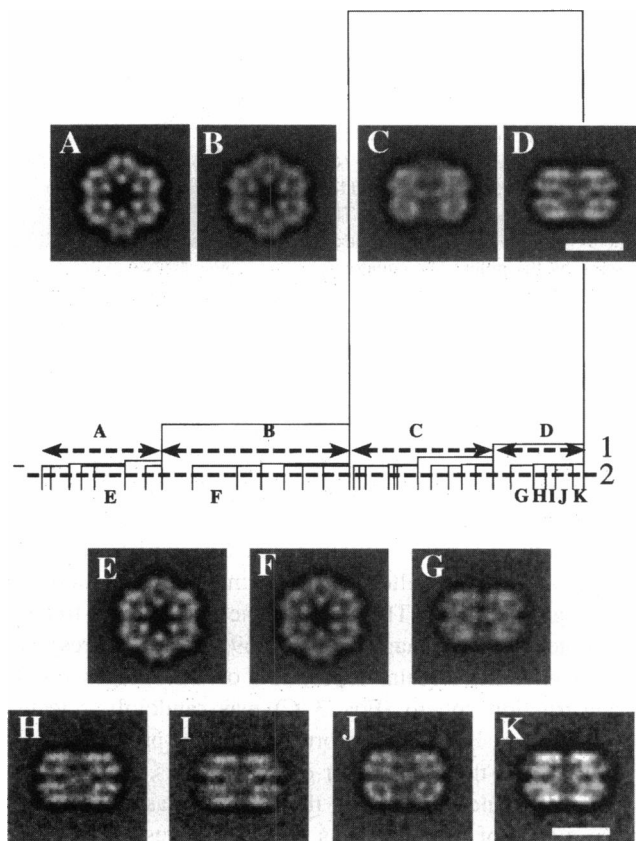

FIGURE 2   Hierarchical ascendant classification of the aligned untilted-specimen images, using Ward's merging criterion (Ward, 1963). The dendrogram cut at the first level (*dashed line no. 1*) produces four images classes whose average maps are shown in *A–D*. At the second cutting level (*dashed line no. 2*) 33 homogeneous smaller image classes are obtained. Of these 33 classes, seven were selected for the reconstruction of the seven primary 3D volumes. Their average images are shown in *E–K*. The scale bars represent 20 nm.

To test this assumption, a test based on the correlation coefficient between the volume in its original position and the same volume rotated around an axis located in its equatorial plane was carried out (see Materials and Methods). The correlation coefficient reached a maximum value of 0.96 every 60°, demonstrating that *Macrobdella* hemoglobin is very close to having a perfect D_6 point-group symmetry. Therefore, the merged 3D reconstruction procedure was repeated with an enforced D_6 point-group symmetry and was further refined by the method of 3D projection alignment. At this stage, the remaining tilted specimen images were included in the process, and three cycles of refinement were carried out until no further improvement could be detected.

As shown in Fig. 3 *A*, the intermediate views used to calculate the 3D reconstruction volume were frequent, whereas the top and side views projecting in the poles and equator of the reconstruction sphere were rare. Conversely, the 613 untilted specimen images extracted from the second series of micrographs that had not been used in the 3D

FIGURE 3 Schematic representation visualizing the orientations used for the 3D reconstruction. (A) The 955 tilted-specimen images. (B) The 613 untilted-specimen images. (C) The subset of 695 images selected for an even angular repartition. The spheres are viewed along an axis passing by the poles. The equator is on the periphery of the circle.

A   **B**   **C**
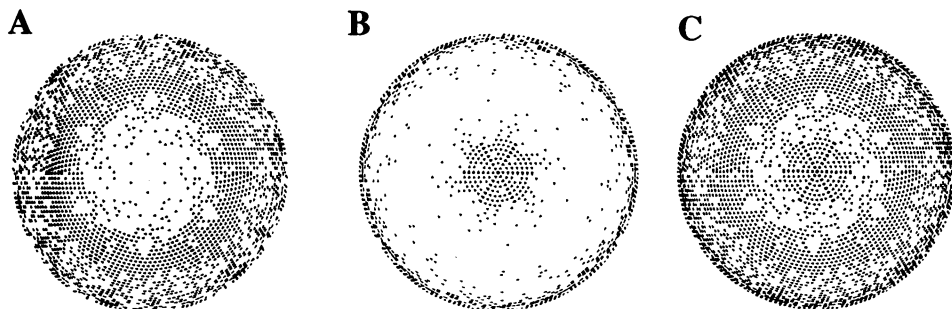
reconstruction mainly contained top and side views. As shown in Fig. 3 B, these images correlate with projections of the volume located in the pole and equator areas of the reconstruction sphere, which are almost devoid of images. To fill in the missing orientations, the 613 untilted specimen images and the 955 tilted specimen images were combined in a single image set. Then, to give the same weight to all of the projections, an image subset of 695 images corresponding to an even angular repartition of the images on the reconstruction sphere (Fig. 3 C) was randomly selected. When several EM images corresponded to projections differing by less than 2° in their φ and θ angles, only one was selected at random. Finally, the volume was submitted to three cycles of refinement as above. The resolution limits estimated on the final volume correspond to 43.2 Å with the DPR and to 40.2 Å with Fourier shell correlation methods, and the final reconstruction volume was filtered down to the resolution limit of 40.5 Å.

Surface representations of the whole molecule

Thresholding strategy

The appearance of the volume depends considerably on the threshold used for the surface representation. In this work, we first chose to represent the volume at a threshold of 100% of the expected molecular volume (4.338×10^6 Å³) calculated on the basis of a molecular mass of 3.56 MDa (Kapp et al., 1990) and of a partial specific volume of 0.734 ml/g (Weber et al., 1995). In the solid-body surface representation calculated by this method, many structural features looked eroded. On the other hand, the distribution of the voxel densities was bimodal, with the higher and lower peaks corresponding to the ice and the protein, respectively (Fig. 4). The function of the threshold being to transform the distribution of the densities into a binary distribution by assigning values of 1 to the protein and 0 to the ice, the threshold must be located between the two peaks. This method, applied to the histogram of Fig. 4, produced a threshold value (0.491) leading to a surface representation where the expected structural details were correctly represented. For comparison, the arrow in Fig. 4 indicates the threshold value deduced from the molecular volume (0.624). The origin of the discrepancy between the two values being unclear, we shall use the value drawn from the

voxel distribution (0.491) for thresholding the volume, even though this volume represents 8.27×10^6 Å³, i.e., 1.9 times the volume calculated from the expected molecular volume. This value is further designated as *normal* threshold and the corresponding volume the *normal* volume.

Overall shape of the 3D volume

The surface representation of the reconstruction volume of *Macrobdella* hemoglobin is shown in Fig. 5 at normal threshold. The molecular architecture shares many features with those of *E. vancouverii* chlorocruorin (de Haas et al., 1995) and *L. terrestris* erythrocruorin (Schatz et al., 1995; de Haas et al., unpublished data). Therefore, architectural terms such as "connections" and "HGS" derive from the nomenclature previously used for the description of the chlorocruorin molecule (de Haas et al., 1995). In the top view orientation (Fig. 5 A), the HBL molecule appears to be composed of two roughly superposed hexagonal layers and a central structure linked to the hexagonal layers (termed a *hexagonal toroid*). The vertex-to-vertex diameter of the molecule is 31.8 nm and its height is 21.1 nm. Each hex-
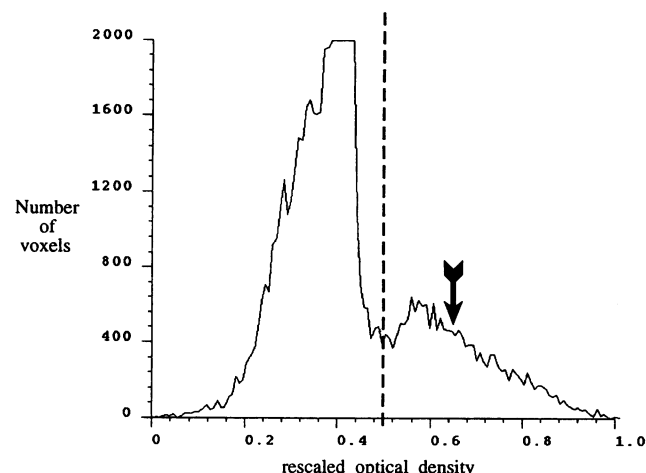

FIGURE 4 Histogram of the voxel densities of the 3D reconstruction volume. The optical densities have been rescaled on a 0.0–1.0 range. The black arrow corresponds to the threshold deduced from the expected molecular volume (0.624). The vertical dashed line corresponds to the normal threshold used throughout this paper (0.491).
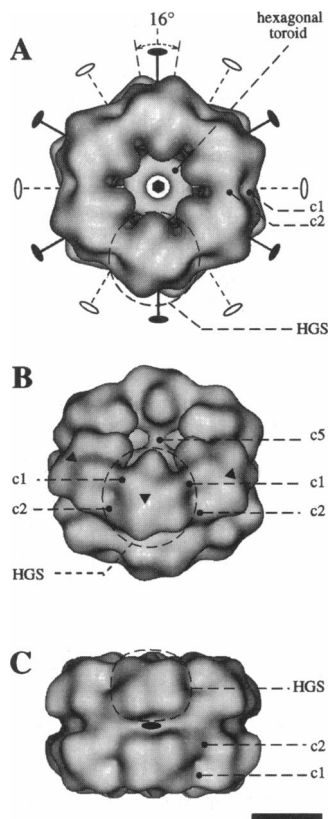
FIGURE 5 Surface representations of *Macrobdella decora* hemoglobin at the normal threshold. (*A*) Top view; (*B*) 45° oblique view; (*C*) side view. The two- and sixfold axes are shown in *A*. Notice that the vertices of the upper and lower hexagonal half-molecules are not superimposed on the twofold axes, the upper hexagonal layer being rotated clockwise around the sixfold axis. A dashed black line circles one HBL. The local pseudo threefold axes of symmetry are marked by black triangles in *B*.

agonal layer comprises six identical HGSs (*dashed circles*) presumed to contain the dodecameric subunit defined by biochemists. The term "HGS" was preferred to the more conventional term "dodecamer," because the dodecamer of globin chains does not account for the totality of the HGS. In the molecule seen along the sixfold axis (Fig. 5 *A*) the vertices of the upper and lower hexagonal layers are not eclipsed, nor are they superimposed on the twofold axes. This disposition, also found in *Eudistylia* chlorocruorin (de Haas et al., 1995), results in an apparent 16° clockwise rotation of the vertices of the upper layer compared to those of the lower layer.

The internal architecture at normal threshold

Starting from the top view (Fig. 5 *A*), a 45° rotation around a horizontal axis brings the volume into such an orientation that it is now viewed along the local pseudo threefold axis of the HGS closer to the observer (Fig. 5 *B*, *black triangles*). This axis that appears more distinctly at higher thresholds will be described under Surface Representation at Higher Thresholds, below. Fig. 5, *A* and *B*, also shows that in each

hexagonal layer the HGSs are in contact with their neighbors via two contact zones termed c1 and c2, which will be more easily visible at higher thresholds. The c1 contact zone is located 3.9 nm above c2 in the upper half-molecule and 6.8 nm above the central plane at a radius of 11.1 nm from the sixfold axis. Also visible in Fig. 5 *B* in the central opening of the HBL is one of the 12 c5 connections between the hexagonal toroid and the HGSs. The side view orientation shows the narrow equatorial area with an external diameter of 26 nm, between the two HGS layers (Fig. 5 *C*).

Fig. 6 shows *Macrobdella* hemoglobin cut along its sixfold axis in two different orientations. As indicated in Fig. 6, *A* and *C*, the cutting planes producing the half-molecules shown in Fig. 6, *B* and *D*, pass between and through neighboring HGSs, respectively. Fig. 6, *B* and *D*, shows that the hexagonal toroid is linked by c5 connections to the internal wall of the HGSs located above and below it. Fig. 6 *D* also shows that at normal threshold the internal cavity of the HGS looks closed and completely isolated from the solvent. In the sections located on the sides of the half-molecule (Fig. 6, *B* and *D*) the various types of connections described below are circled with dashed lines.

Organization of the HGSs

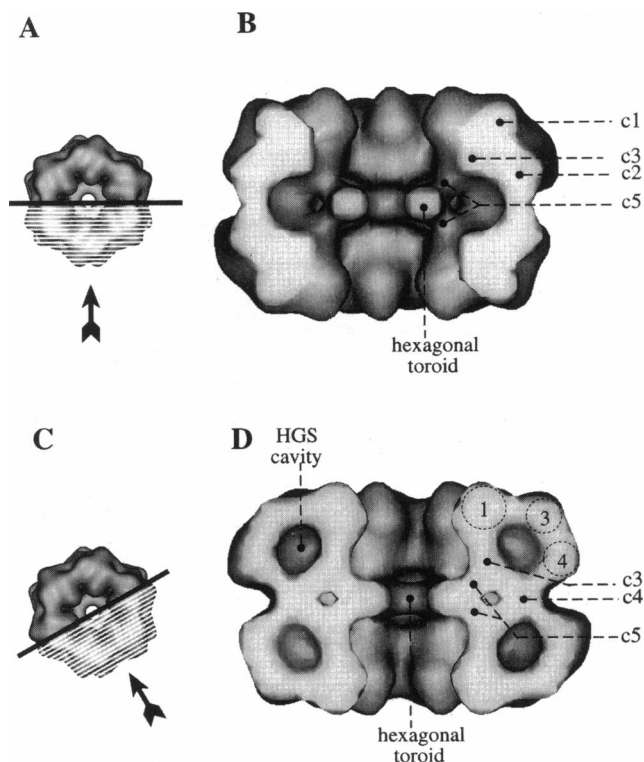Schematically, in the HBL viewed along one of its twofold axes and from inside the volume, the HGS appears to be

FIGURE 6 Surface rendering at the normal threshold of the 3D reconstruction volume of *Macrobdella decora* hemoglobin cut in half by a plane passing by the sixfold axis. The cutting plane passes between (*A*, *B*) and through (*C*, *D*) neighboring HGSs. The hatched parts of the molecule are removed and the directions of observation are indicated by an arrow.

composed of a ceiling, a floor, and four walls (one external, one internal, and two lateral). The shape of the internal wall (Fig. 6 B) suggests that it may comprise two parts, an upper globular portion, termed mass no. 1 (see Fig. 9 for the location of masses 1 through 6), and a lower part, termed the c3 connection body, extending to the neighboring HGSs. The lateral walls are composed of c1, c2 contact zones, and the ends of the c3 connections (Fig. 6 B). The external wall comprises five masses, designated as masses 2 through 6, which separate from each other only at high threshold. In the section of Fig. 6 D, the cutting plane passes through masses N°3 and 4 (see Fig. 6 C for the orientation of the cutting plane). The floor of the HGS corresponds to the c4 connection body and the ceiling to the contact zone between mass N°1 of the internal wall and masses N°2 and 3 of the external wall.

As shown in Fig. 7, sectioning the whole molecule perpendicularly to its sixfold axis allows a better view of the floor and the ceiling of the HGS cavity. Fig. 7, A and C, shows the cutting levels and the observation direction (arrows) of the volume fragments shown in Fig. 7, B and D, respectively. Fig. 7 B shows the upper third of the upper hexagonal layer, viewed from below. The cutting plane passes through the c3 connection bodies and through masses 4, 5, and 6. As described above, the ceiling of the cavity is completely closed. The tops of the six internal walls (mass 1) are also easily visible, protruding in the central opening of the volume. Fig. 7 D shows the lower third of the upper hexagonal layer. It can be easily observed that the hexagonal toroid is connected to the HGS internal walls by c5 connections and that the thicker external walls are composed of masses 4, 5, and 6. It is clear from Fig. 7 D that the vertices of the hexagonal toroid are located almost perfectly on the twofold axes (Fig. 7 D, dashed line). The floors of the HGS cavities, made up of the top of the c4 connection bodies located underneath, are not perforated at normal threshold.

Surface representations at higher thresholds

Thresholds displaying 65% and 47% of the normal volume

When eroding the 3D volume by raising the threshold, the areas with the highest densities become progressively more resolved. As shown in Fig. 8, A and B, when 65% of the normal volume is left apparent the HGSs progressively individuate. The c1 and c2 contact zones appear now as
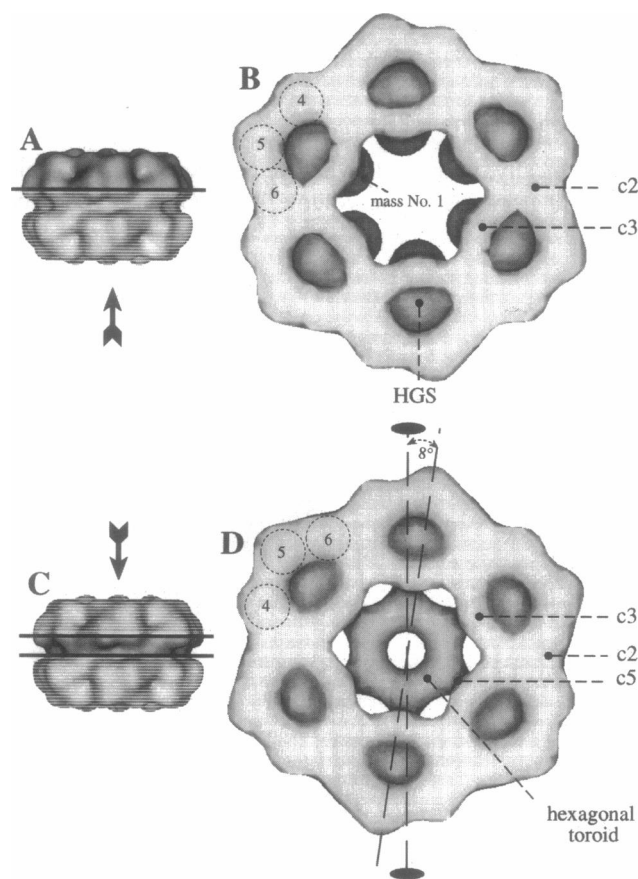

FIGURE 7 Solid-body surface representation of the 3D reconstruction volume of *Macrobdella decora* hemoglobin cut perpendicularly to the sixfold axis. The cutting planes represented by the black horizontal lines pass through the ring of c3 connections (in A and B) and through the hexagonal toroid (in C and D). The hatched parts of the molecule are removed and the directions of observation are indicated by arrows. (B) The upper two-thirds of the upper hexagonal layer of the molecule viewed from below. As indicated in the left part of the figure (arrow), this view shows the ceiling of the HGS cavities. (D) The lower third of the upper hexagonal layer of the molecule viewed from above.
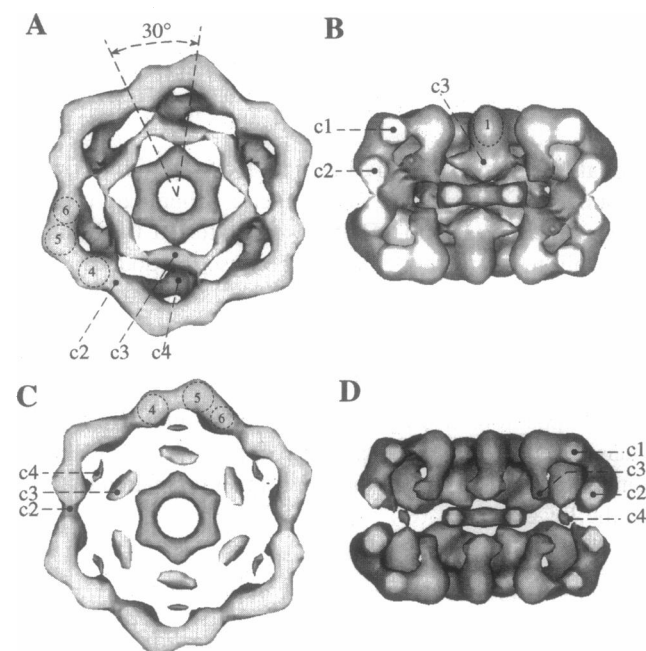

FIGURE 8 Solid-body surface represention of the 3D reconstruction volume of *Macrobdella decora* hemoglobin cut perpendicularly (A, C) and parallel (C, D) to the sixfold axis, at thresholds of 65% (A, B) and 47% (C, D). The positions of the cutting planes in A and C are the same as in Fig. 7 C. The positions of the cutting plane in B and D are the same as in Fig. 7 A.

short cylinders ~2.9 nm in diameter located at radii of 11.1 and 11.8 nm and at distances of 6.8 and 2.9 nm from the equatorial plane, respectively. The two lateral walls of the HGS have disappeared (see the sections of the HGS located in both sides of Fig. 8 *B*). The architecture of the internal wall of the HGS is now clearer, with an upper globular structure (mass 1) and a lower ovoid body, the c3 connection body, extending to the neighboring HGSs (Fig. 8 *B*). In a previous report on the structure of *Eudistylia* chlorocruorin (de Haas et al., 1995), the structure comprising mass 1 and the c3 connection body was termed "the *loop body* of the HGS." In the present paper, we shall use another denomination termed the "internal wall of the HGS." In each half-molecule, the c3 connection bodies of the six HGSs come into contact and make an internal hexagonal bracelet located at a radius of 3.6 nm from the sixfold axis and at a distance of 3.9 nm from the central plane. The vertices of the hexagonal bracelet are rotated ~30° compared to those of the hexagonal layer and of the hexagonal toroid (Fig. 8 *A*). Because of the erosion, two holes in the HGS floor open the cavity to the outside environment (small external hole) and to the internal compartment of the HBL structure (large elongated hole). The remaining material of the floor comprises the c4 connection body (located near the equatorial plane at a radius of 10.3 nm from the sixfold axis) and its three arms bound to the c3 connection body and to masses 4 and 6 (Fig. 8 *A*). In fact, each c4 connection body possesses six arms, three being bound to each of the two HGSs located below and above it.

At a threshold displaying 47% of the normal volume i) the c4 connection bodies are reduced to six small densities (Fig. 8 *C*); ii) the bracelets of c3 connections are fragmented (Fig. 8, *C* and *D*), and the c3 connection bodies represent only small globular expansions at the end of the loop bodies (Fig. 8 *D*); iii) the hexagonal toroid is disconnected from the HGSs; and iv) the c1 and c2 contact zones are still present, although considerably reduced.

Thresholds displaying 26% and 13% of the normal volume

Raising the threshold so that 26% of the normal volume remains shows that the c1 and c2 contact zones break and that the HGSs become completely separated (Fig. 9, *A*, *C*, *E*). At this threshold, the HGS appears to be composed of six approximately globular masses (numbered 1 through 6) that are still partially fused. Mass 1, corresponding to the upper globular portion of the internal wall (Fig. 9 *A*), is connected to mass 2 by a large bridge, making the group of masses 1 + 2 resemble a dumbbell. The external wall of the HGS comprises five masses (Fig. 9 *C*), two on the top (2 and 3) and three on the bottom (4 to 6). The protrusion of the six masses (no. 5) on the outside of the molecule correspond to the vertices of the HBL. Continuing to erode the volume down to 13% of the normal volume leads to the disappearance of the connections between masses 2 and 5 and between masses 4 and 5 (Fig. 9, *B*, *D*, and *F*). At this threshold, the HGS seems to be composed of three elon-
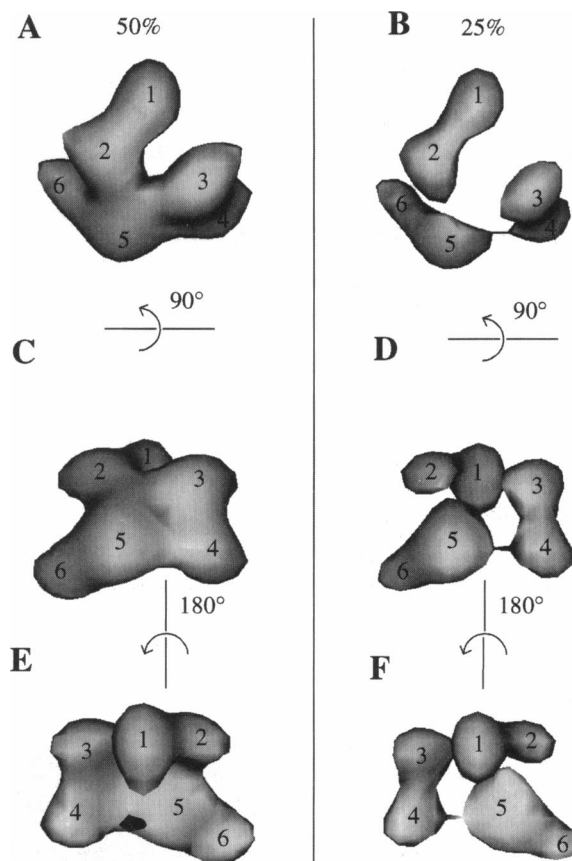

FIGURE 9 Surface rendering of a substructure obtained by raising the threshold to such a level that 26% (*A*, *C*, *E*) and 13% (*B*, *D*, *F*) of the normal volume are left apparent. To simplify the description, six high-density masses are labeled 1 through 6. In *B*, *D*, and *F* the structure separates into three elongated structures, the first two being dumbbell-shaped (1–2 and 3–4) and the third (5–6) remaining compact.

gated bodies comprising masses 1 + 2, 3 + 4, and 5 + 6, respectively. A further increase of the threshold leads to the separation of masses 1 and 3 from masses 2 and 4, respectively, but not of masses 5 and 6, which do not separate, even for thresholds as high as 99%.

The disposition of the three elongated structures suggests that they may be related by a local pseudo threefold symmetry, as in *Lumbricus* (Schatz et al., 1995) and *Eudistylia* (de Haas et al., 1995). To test for this symmetry, six spheres were superposed at best on masses 1 through 6, and a threefold axis bringing the spheres into coincidence was searched for. The best axis cuts the sixfold axis 7.4 nm below the center of the molecule and makes a 49° angle with the sixfold axis. However, the observed threefold symmetry seems imperfect. For example, masses 1 and 5 are larger than masses 2 and 6, respectively. Also puzzling is the fact that masses 5 and 6 do not dissociate, even at very high threshold, whereas masses 1–2 and 3–4 do. These features may be due to an imperfect threefold symmetry or to the absence of correction of the CTF.

In contrast to the central flat disk observed in *Eudistylia* chlorocruorin the hexagonal toroid of *Macrobdella*, hemo-

globin starts to dissociate into six separate masses when the volume is eroded down to 30% of the normal volume. At a threshold leaving an apparent 20% of the normal volume, only the six small masses resulting from the fragmentation of the toroid and masses 1 through 6 of the HGSs remain.

Internal organization of the volume

Sections parallel to the sixfold axis

Understanding the internal structure of the molecule is greatly simplified by cutting through the 3D volume two series of slices parallel (Fig. 10, *B1* to *B6*) and perpendicular (Fig. 10, *D1* to *D6*) to the sixfold axis. The positions of the cutting planes and the direction of observation corresponding to Fig. 10, *B* and *D*, are represented in Fig. 10, *A* and *C*, respectively. As indicated in Fig. 10, *A1* and *C1*, for the sake of convenience the HGSs of the upper and lower hexagonal layers are labeled *a* through *f* and *a'* through *f'*. In slice 10 *B1*, which cuts HGSs *b*, *b'*, *a*, *a'*, and *f*, *f'*, the two dark zones correspond to the internal cavities of HGSs

a and *a'*. Slice 10 *B2* shows i) the central cavities of HGSs *b'* and *f* (the dark zones in the upper-right and lower-left corners), ii) the external wall of HGSs *b* and *f'*, and iii) the loop bodies of HGSs *a* and *a'* (the white spots close to the vertical median line). Slice 10 *B3* passes through the internal cavities of four HGSs (*b*, *b'*, *f*, and *f'*), producing four dark spots. In addition, three high-density spots are visible near the vertical median line. As above, the upper and lower spots correspond to the vertical loop bodies of HGSs *a* and *a'* and the central spot to the section of one vertex of the hexagonal toroid. The structure of the hexagonal toroid is also easily understood from Fig. 10 *B4*, where the four c5 connections linking the toroid to the four HGSs located at the four corners are easily visible. In the HGSs located in the upper right and lower left areas, the cutting plane passing on the outer side of masses 1, 3, and 4 (see Fig. 9), the top of the cavity looks open. Fig. 10 *B5* is more complex to interpret. The two densities located in the middle of the slice obviously correspond to the hexagonal toroid. The two pairs of high-density nuclei located near the horizontal median axis on the left and right sides of the slice correspond to masses 6 of HGS *b*, *c'*, *e*, and *f'*. The four nuclei disposed on the vertical median axis correspond from top to bottom to the internal walls of HGSs *d* and *d'*. In addition, the HGSs located at the four corners of the slice appear as groups of triangularly disposed densities corresponding to the wall (masses 3 and 4 or 2 and 6 plus c1 and c2 contact zones) and to the c3 connexion body of HGSs *c*, *c'*, *e*, and *e'*. Finally, because of the D_6 point-group symmetry and the imperfect eclipsed disposition of the hexagonal layers, the last slice (Fig. 10 *B6*) is identical to the mirror-inverted slice 10 *B3*, with the upper density of the vertical median line slightly shifted to the right compared to the lower one.

Sections perpendicular to the sixfold axis

The sections of Fig. 10 *D* are favorable to the observation of the masses composing the HGS. The first slice (Fig. 10 *D1*) only contains the upper portion of masses 1, 2, and 3 of each HGS. Then, Fig. 10 *D2* shows masses 1, 2, and 3 and the top of masses 4 and 5–6. The opening between masses 1 and 3 has already been encountered in Fig. 9 *A*. In slice 10 *D3*, one distinctly sees the lower part of the HGS with the wall masses (nos. 4 and 5–6) and the bracelet of c3 connections (compare with Fig. 7 *B* or 8 *A*) limiting the six HGS internal cavities. Slice 10 *D4* shows the floor of the HGS internal cavity (compare with Figs. 7 *D* and 8 *A*). Slice 10 *D5* contains the region located exactly between the two hexagonal layers, with the central hexagonal toroid and the peripheral c4 connections area. Finally, Fig. 10 *D6* shows a slice through HGSs *a'* to *f'*, which is homologous but mirror inverted when compared to slice of Fig. 10 *D3*. This is due to the 16° clockwise rotation of the vertices of the upper hexagonal layer (slice 10 *D3*) with respect to those of the lower layer (slice 10 *D6*).
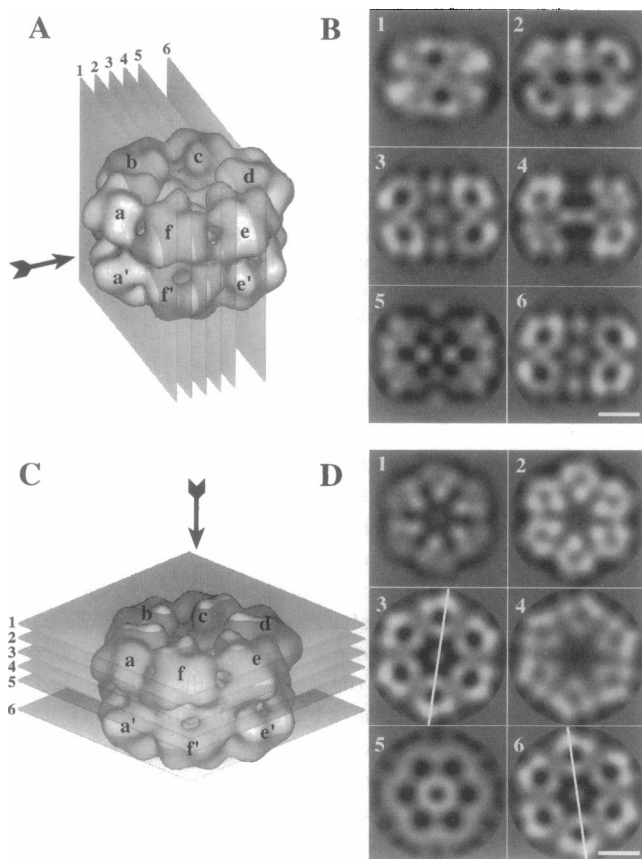
FIGURE 10   Shaded surface representation (*A*, *C*) and slices (*B*, *D*) through the reconstruction volume parallel (*A*, *B*) and perpendicular (*C*, *D*) to the sixfold axis. The upper and lower dodecamers are labeled *a* to *f* and *a'* to *f'*, respectively. Planes A1 through A6 correspond to slices B1 through B6, respectively, and planes C1 to C6 correspond to slices D1 to D6. The black arrows indicate the observation directions. The length of the bar is 10 nm.

Comparison of the refined 3D reconstruction volume to experimental average images

To study the validity of the refined 3D reconstruction volume, one of the best quality criteria is to check whether the 3D volume can produce 2D projection maps resembling the original cryoelectron microscopy 2D average images. In this work, for all 33 image clusters we could always find a projection of the 3D volume in excellent agreement with the authentic average image. Fig. 11 shows a selected set of six pairs of average images and projection maps corresponding to the three main types of EM views. Obviously, the excellent agreement demonstrates that the reconstruction volume is very similar to the authentic molecules.

DISCUSSION

Choice of a threshold

As stated above, the appearance of the 3D volume essentially depends on the threshold used for the surface render-
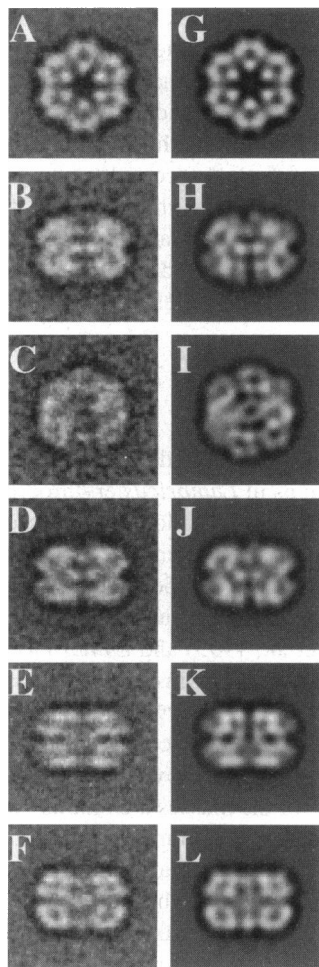

FIGURE 11   Comparison of some projections of the 3D reconstruction volume of *Macrobdella decora* hemoglobin with authentic two-dimensional average maps. *(A–F)* Average images; *(G–L)* 2D projection maps of the 3D reconstruction volume calculated by integrating the densities along the directions of projection.

ing. There are two possible approaches to determining the threshold of the native molecule; the first one relies on the distribution of the voxel optical densities, the second on the molecular volume computed from the molecular mass and the partial specific volume. The problem is that the two methods provide different threshold values. With *Macrobdella* hemoglobin these methods allowed us to see 18,194 and 9,544 voxels (8.27 and 4.34 $\times$ 10^6 Å^3), respectively. The first threshold is obviously too high in terms of absolute volume value for the native molecule, but the volume calculated from second value is obviously too eroded. The cause of this phenomenon is that a 3D reconstruction is not an absolute representation of the original molecule, but an approximation of its structure calculated from a set of imperfect images. Hence, the limitations inherent in all electron microscopes, especially the CTF imposing a band pass in low- and high-spatial frequencies, introduce a spreading of the densities within the 3D reconstruction volume. Frank et al. (1991) explain that the threshold of a 3D reconstruction volume corresponds to "a median boundary within a shell of uncertainty." In this context the threshold estimated from the exact molecular volume of the particle does not apply to the 3D reconstruction. The difference in the threshold values may also be due to the fact that at limited resolution many small cavities are not resolved and thus are interpreted as mass. Therefore, in a reconstruction from frozen-hydrated specimen, a method that induces no drying artifact and shrinkage of the particles, the envelope of the structure determined by a given threshold value should include a larger volume than predicted by molecular mass. It follows that the threshold inferred from the optical density distribution gives a correct qualitative estimate of the boundary between the protein and the vitreous ice, even though it is not a good quantitative estimate of the real size of the particle.

In practice, we compared the relative volumes of various fragments, expressed as a percentage of the total 3D volume; then we transformed these results into molecular mass, supposing that the 3D volume is isotropic and the fragments have similar partial specific volumes. Despite these restrictions, this method gave results in good agreement with the available experimental data collected by other methods such as mass spectrometry or x-ray crystallography.

The handedness of the whole oligomer

As visible in the molecule from its top view, the vertices of the upper half-molecule are rotated 16° clockwise with respect to their homologs in the lower half-molecule (Fig. 5 *A*). If we define molecular architectures with the upper half-molecule rotated clockwise and counterclockwise as right- and left-handed isomers, respectively, then the 3D volume of *Macrobdella* hemoglobin is right-handed. The same architecture with an angle of 14°, instead of 16°, was observed recently in *E. vancouverii* chlorocruorin (de Haas et al., 1995) and in *L. terrestris* hemoglobin (de Haas et al.,

unpublished data). Recently, a 3D reconstruction volume of *Lumbricus* hemoglobin was computed with the angular reconstruction method from a frozen-hydrated sample (Schatz et al., 1995). As this method does not require the specimen to be tilted, the authors did not determine the correct handedness of the reconstructed particle and the (wrong) left-handed enantiomer was presented throughout the paper. The choice of the correct enantiomer in symmetrical structures is clearly a limitation of the angular reconstitution method of Van Heel (1987).

The role of the hexagonal toroid

In contrast to *Eudistylia* chlorocruorin and *Lumbricus* erythrocruorin (Schatz et al., 1995; de Haas et al., unpublished data), where the center of the molecule is occupied by a flat hexagonal mass, the central region of *Macrobdella* hemoglobin contains a hexagonal toroid. The structural role of the toroid is obviously to be a pier to which the two bracelets of c3 connections are fixed by 12 c5 connections. The volume of the hexagonal toroid determined by masking the HGSs represents 4.4% of the volume of the whole molecule corresponding to a total molecular mass of 157 kDa, i.e., six 26.2 kDa linker chains. Moreover, upon progressive erosion of the volume by raising the threshold, the hexagonal toroid fragments into six substructures, as expected with a hexameric structure. Because of its keystone position the hexagonal toroid may be involved in the cooperative oxygen binding. Indeed, annelid hemoglobins possess at least two levels in the cooperativity, a first level depending on the integrity of the dodecamer and a second one requiring the presence of the linker chains. The hexagonal toroid with or without the c3- and c4 connections would be an excellent candidate for being involved in the second level of cooperativity. From an evolutionary point of view it would also be interesting to know whether a toroid is present in all of the achaete hemoglobins and only in those hemoglobins and to search for a difference in the functional properties related to the toroid structure.

The linker chains and the quaternary structure of the hemoglobin molecule

Macrobdella hemoglobin, as other annelid hemoglobins, is composed of 12 dodecamers of a ~17 kDa globin chain and 30 to 40 heme-deficient ~30 kDa linker chains belonging to at least three polypeptide types (Kapp et al., 1990). Recently, on the basis of mass spectrometeric measurements, Weber et al. (1995) established that the proportions of the three linker chains that they separated (peaks C, D, and E) were 1/6/3, respectively. Besides the subunit composition, we also know by the present 3D reconstruction that the whole oligomer comprises 12 copies of a repeating HGS with a local pseudo threefold symmetry cross-linked by a complex system of connections. In this system, the c1 and c2 contact zones do not require the presence of linker chains

between them. Indeed, masses 2 and 3 on the one hand and 4 and 6 on the other hand are close enough to be involved in noncovalent protein-protein interactions, possibly involving calcium ions. Besides the c1 and c2 contact zones, three additional types of interconnected structures that we propose to define as the linker complex (i.e., the hexagonal toroid, the c3-, and the c4 connections) strengthen the molecule and might be involved in the cooperative oxygen binding. The proportions of the linkers obtained by mass spectrometry are different enough to try to identify them in our 3D reconstruction volume by comparing the volume of the structural elements calculated as described above (see Choice of a Threshold, above). Thus it has been shown above that the hexagonal toroid represents 4.4% of the total volume. For the c3 and c4 connections this estimation was more difficult because at normal threshold they are more intricately associated with the rest of the molecule. However, by sectioning the molecules with parallell planes or spheres and by masking the unwanted structures we obtained a satisfactory evalution of their volumes. Thus, the two bracelets of c3 connections represented 14.6% of the normal volume and the six c4 connections 7.92%. If we impose the requirement that the number of each linker chain must be a multiple of 6, then the c3 connection represents 24 linker chains of 21.65 kDa and the c4 connection 12 linker chains of 23.5 kDa. Given the difficulty of isolating the various portions of the linker complex, these proportions are in acceptable agreement with the data of Weber et al. (1995), and we can propose that the linkers corresponding to peaks C, D, and E correspond to the hexagonal toroid, the c3, and the c4 connections, respectively.

The HGS in detail

It does not appear that stable dodecamers occur in *Macrobdella* hemoglobin as in *Lumbricus* erythrocruorin (Weber et al., 1995). Conversely, the dodecamers seem to be composed of tetramers in equilibrium with their monomeric and disulfide-linked dimeric components. On the other hand, in this and in other 3D reconstructions carried out with *Eudistylia* (de Haas et al., 1995) and *Lumbricus* (de Haas et al., unpublished data) hemoglobins, the 12 HGSs have the same architecture, with an external wall (masses 2 through 6), an internal wall (mass 1 and c3 connection body), and a floor (c4 connection body). Moreover, in the three species, the relative positions of the masses are similar, with masses 1 + 2 and 3 + 4 associated in dumbbell-shaped structures and masses 5 + 6 grouped in an elongated compact mass. Therefore, one can conclude that i) each elongated structure contains four globin chains linked or not by disulfide bonds, ii) the compact structure (masses 5 + 6) is organized differently from the other two, and iii) this organization is independent of the polymerization degree of the globin chains (monomers, dimers, trimers, or tetramers). Another important particularity of the HGS is the presence in the three species of a pseudo threefold axis of symmetry, mak-

ing an angle of ~45° with the sixfold axis. Two successive 120° rotations around this axis bring into approximate co-incidence masses 2, 3, and 5 on the one hand and 1, 4, and 6 on the other hand. The fact that this symmetry concerns the three functional elongated structures but not the c3 connection bracelet made up of linker chains is highly relevant.

Recently, Martin et al. (1996a) have crystallized do-decamers isolated from *Lumbricus* erythrocruorin. These authors, assuming that the asymmetric unit contains an entire dodecamer, concluded from the symmetry of their crystal that the 12 globin chains are roughly coplanar and form a 69.5-Å-thick single layer with a pseudo threefold symmetry. They also suggested that, although in their crystal the dodecamer is flat, in the native structure it could take a 140-Å-thick domed-up configuration "in which the 3-fold symmetry and the trimer-to-trimer contacts are preserved." This domed-up configuration used in their companion paper (Martin et al., 1996a) is in perfect agreement with the disposition of masses 1 through 6 observed in the HGSs of *Eudistylia* chlorocruorin (de Haas et al., 1995) and in *Macrobdella* (this paper) and *Lumbricus* (Schatz et al., 1995; de Haas et al., unpublished data) erythrocruorins.

A model of *Macrobdella* erythrocruorin

The major part of the model shown in Fig. 12 comprises 12 dodecamers with a threefold symmetry (Fig. 12 *A*). Each dodecamer is composed of three masses, each representing a tetramer and corresponding to masses 1 + 2, 3 + 4, and 5 + 6 observed in *Macrobdella*, *Eudistylia*, and *Lumbricus* hemoglobins. The masses are disposed as in the domed-up model of Martin et al. (1996a). The second building block is the hexagonal toroid. It is composed of six copies of a linker chain, each linked to a pair of HGSs by two c5 connections. We arbitrarily assigned the c5 connections to the toroid, but they could as well belong to c3 connection bodies (Fig. 12 *B*). The third structural element comprises the two bracelets of c3 connections and accounts for 24 copies of linker chains. Each bracelet is linked to mass 1 of six dodecamers, to the inner arm of the c4 connection body, and to six C5 connections of the hexagonal toroid (Fig. 12 *C*). The last element, the c4 connection, is present in six copies and accounts for the floor of the HGS by its body and its three arms (Fig. 12 *D*). Again, we ignore whether the c4 connection body and arms belong to the same linker chain. Upon eroding the volume the arms disappear before the body, so that they could belong to the neighboring structures as well. Fig. 12 *E* shows the assembly of the toroid plus the c3 and c4 connections, which we term the linker complex, and Fig. 12 *F* the whole hexagonal bilayer molecule.

This model has in common with the model of Weber et al. (1995) i) a composition of 144 globin chains and 42 linker chains, ii) the D6 point-group symmetry of the HBL, iii) the local threefold axes of the dodecamers, and iv) the domed-up organization of the dodecamer. The main differ-
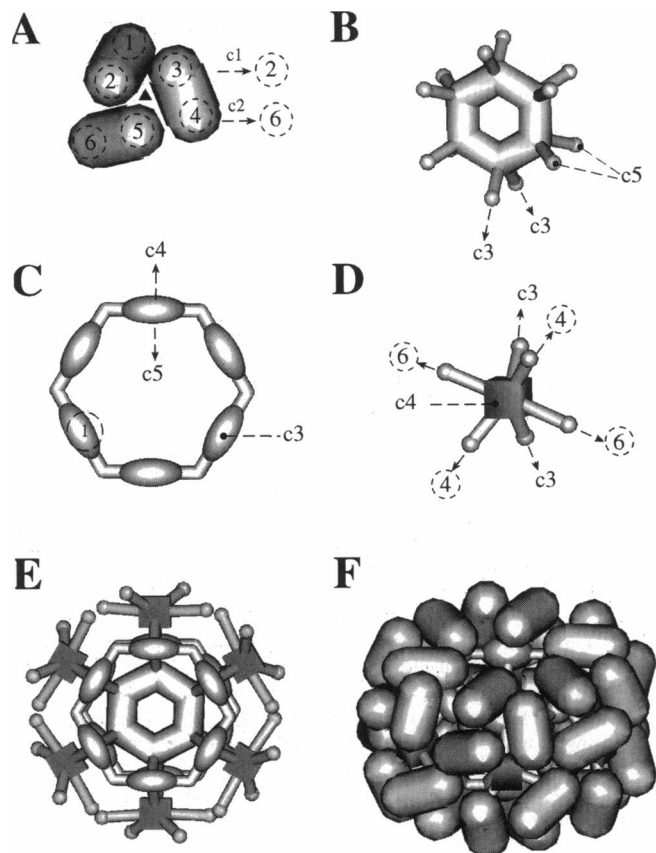

FIGURE 12 Model of architecture of *Macrobdella decora* hemoglobin derived from the present 3D reconstruction volume. (*A*) The dodecamer; (*B*) the hexagonal toroid with the c5 connections; (*C*) the bracelet of c3 connections; (*D*) a c4 connection; (*E*) the linker complex; (*F*) the entire HBL molecule. To avoid the complete masking of the linker complex by the dodecamers, the tetramers of globin chain are represented smaller than in the real volume. The numbers circled by dashed lines in *A*, *C*, and *D* correspond to the masses described in Fig. 9.

ences are the organization of the linker complex and the distribution of the linker chains between the various types of connections.

CONCLUSION

The 3D reconstruction volumes obtained from the random conical tilt series method applied to frozen-hydrated specimens of *M. decora*, *E. vancouverii*, and *L. terrestris* hemoglobin possess similar architectures. Clearly, all of the annelid hemoglobins studied so far possess a unique architecture based on a right-handed structure. The HGS architecture is also remarkably constant, in view of its variable degree of aggregation (monomers, dimers, trimers, or tetramers). Indeed, in the three species the dodecamer comprises three elongated structures related by a pseudo threefold symmetry, one of them being more compact than the other two at higher thresholds. The linker complex is also remarkably similar, with a hexagonal central mass, two bracelets of c3 connections, and six c4 connections. Only

minor differences, such as the presence of a hole in the central mass or a slightly different structure of the c4 connection, could be found.

REFERENCES

Adrian, M., J. Dubochet, J. Lepault, and A. W. McDowall. 1984. Cryo-electron microscopy of viruses. *Nature.* 308:32–36.

Antonini, E., and E. Chiancone. 1977. Assembly of multisubunit respiratory proteins. *Annu. Rev. Biophys. Bioeng.* 6:239–271.

Boekema, E. J., and M. Van Heel. 1989. Molecular shape of *Lumbricus terrestris* erythrocruorin studied by electron microscopy and image analysis. *Biochim. Biophys. Acta.* 957:370–379.

Boisset, N., P. Penczek, F. Pochon, J. Frank, and J. Lamy. 1993. Three-dimensional architecture of human α_2-macroglobulin transformed with methylamine. *J. Mol. Biol.* 232:522–529.

de Haas, F., J.-C. Taveau, N. Boisset, O. Lambert, S. N. Vinogradov, and J. N. Lamy. 1995. Three-dimensional reconstruction of the chlorocruorin of the polychaete annelid *Eudistylia vancouerii. J. Mol. Biol.* 255:140–153.

Dubochet, J., M. Adrian, J.-J. Chang, J.-C. Homo, J. Lepault, A. W. McDowall, and P. Schultz. 1988. Cryoelectron microscopy of vitrified specimens. *Q. Rev. Biophys.* 21:129–228.

Frank, J., P. Penczek, R. Grassucci, and S. Srivastava. 1991. Three-dimensional reconstruction of the 70S *Escherichia coli* ribosome in ice: the distribution of the ribosomal RNA. *J. Cell. Biol.* 115:597–605.

Frank, J., B. Shimkin, and H. Dowse. 1981a. Spider—a modular software system for electron image processing. *Ultramicroscopy.* 6:343–358.

Frank, J., A. Verschoor, and M. Boublik. 1981b. Computer averaging of electron micrographs of 40S ribosomal subunits. *Science.* 214:1353–1355.

Gotoh, T., and T. Suzuki. 1990. Molecular assembly and evolution of multi-subunit extracellular annelid hemoglobins. *Zool. Sci.* 7:1–16.

Green, B. N., T. Suzuki, T. Gotoh, and S. N. Vinogradov. 1995. Maximum entropy analysis of the electrospray ionization mass spectrometry of the extracellular hemoglobin of *Tylorrhincus heterochaetus. J. Biol. Chem.* 270:18209–18211.

Ilan, E., and J. Haroun. 1993. Oxygen-binding properties of extracellular hemoglobin from the leech, *Hirudo medicinalis.* Effects of pH, cations and temperature. *Biochim. Biophys. Acta.* 1162:77–83.

Kapp, O. H., A. N. Qabar, M. C. Bonner, M. S. Stern, D. A. Walz, M. Schmuck, I. Pilz, J. S. Wall, and S. N. Vinogradov. 1990. Quaternary structure of the giant extracellular hemoglobin of the leech *Macrobdella decora. J. Mol. Biol.* 213:141–158.

Lambert, O., N. Boisset, J.-C. Taveau, G. Préaux, and J. N. Lamy. 1995. Three-dimensional reconstruction of the α_D and β_C-hemocyanins of *Helix pomatia* from frozen-hydrated specimens. *J. Mol. Biol.* 248:431–448.

Lebart, L., A. Morineau, and K. M. Warwick. 1984. Hierarchical classification. *In* Multivariate Descriptive Statistical Analysis. Wiley, New York. 117–143.

Martin, P. D., K. L. Eisele, M. A. Doyle, A. R., Kuchumov, D. A. Walz, E. G. Arutyunyan, S. N. Vinogradov, and B. F. P. Edwards. 1996a. Molecular symmetry of the dodecamer subunit of *Lumbricus terrrestris* hemoglobin. *J. Mol. Biol.* 255:170–176.

Martin, P. D., A. R. Kuchumov, B. N. Green, R. W. A. Oliver, E. H. Braswell, J. S. Wall, and S. N. Vinogradov. 1996b. Mass spectrometry composition and molecular mass of *Lumbricus terrrestris* hemoglobin: a refined model of its quaternary structure. *J. Mol. Biol.* 255:154–169.

Milligan, R. A., A. Brisson, and P. N. T. Unwin. 1984. Molecular structure determination of crystalline specimens in frozen aqueous solutions. *Ultramicroscopy.* 13:1–10.

Misell, D. L. 1978. Image analysis, enhancement and interpretation. *In* Practical Methods in Electron Microscopy, Vol. 7. A. M. Glauert, editor. North-Holland, Amsterdam. 33–90.

Ownby, D. W., H. Zhu, K. Schneider, R. C. Beavis, B. T. Chait, and A. F. Riggs. 1993. The extracellular hemoglobin of the earthworm *Lumbricus terrestris.* Determination of subunit stoichiometry. *J. Biol. Chem.* 268:13539–13547.

Penczek, P. A., R. A. Grassucci, and J. Frank. 1994. The ribosome at improved resolution: new techniques for merging and orientation refinement in 3D cryoelectron microscopy of biological particles. *Ultramicroscopy.* 53:251–270.

Penczek, P., M. Radermacher, and J. Frank. 1992. Three-dimensional reconstruction of single particles embedded in ice. *Ultramicroscopy.* 40:33–53.

Qabar, A. N., M. S. Stern, D. A. Walz, J. T. Chiu, R. Timkovich, J. S. Wall, O. H. Kapp, and S. N. Vinogradov. 1991. Hierarchy of globin complexes. The quaternary structure of extracellular chlorocruorin of *Eudistylia vancouverii. J. Mol. Biol.* 222:1109–1129.

Radermacher, M. 1988. Three-dimensional reconstruction of single particles from random and non-random tilt series. *J. Electron Microsc. Tech.* 9:359–394.

Radermacher, M., T. Wagenknecht, A. Verschoor, and J. Frank. 1987a. Three-dimensional structure of the large ribosomal subunit from *Escherichia coli. EMBO J.* 6:1107–1114.

Radermacher, M., T. Wagenknecht, A. Verschoor, and J. Frank. 1987b. Three-dimensional reconstruction from a single-exposure, random conical tilt series applied to the 50 S ribosomal subunit of *Escherichia coli. J. Microsc.* 146:113–136.

Saxton, W. O., and W. Baumeister. 1982. The correlation averaging of a regularly arranged bacterial cell envelope protein. *J. Microsc.* 127:127–128.

Schatz, M., E. V. Orlova, P. Dube, J. Jaeger, and M. Van Heel. 1995. Structure of *Lumbricus terrestris* hemoglobin at 30 Å resolution determined using angular reconstruction. *J. Struct. Biol.* 114:28–40.

Taveau, J.-C. 1996. Presentation of the Sigma software. Software of Imagery and Graphics for Molecular Architecture. *J. Struct. Biol.* In press.

Taveau, J.-C., and J. Lamy. 1990. Three-dimensional modeling of hemocyanin as a help for the interpretation of electron microscope images. *In* Invertebrate Dioxygen Carriers. G. Préaux and R. Lontie, editors. Leuven University Press, Louvain. 275–278.

Van Heel, M. 1984. Multivariate statistical classification of noisy images (randomly oriented biological macromolecules). *Ultramicroscopy.* 13:165–184.

Van Heel, M. 1987. Angular reconstitution: a posteriori assignment of projection directions for 3D reconstruction. *Ultramicroscopy.* 21:111–124.

Van Heel, M., and J. Frank. 1981. Use of multivariate statistics in analysing the images of biological macromolecules. *Ultramicroscopy.* 6:187–194.

Vinogradov, S. N., O. H. Kapp, and L. Ohtsuki. 1982. The extracellular hemoglobins and chlorocruorins of annelids. *In* Electron Microscopy of Proteins, Vol. 3. J. Harris, editor. Academic Press, New York. 135–163.

Vinogradov, S. N., S. D. Lugo, M. G. Mainwaring, O. H. Kapp, and A. V. Crewe. 1986. Bracelet protein: a quaternary structure proposed for the giant extracellular hemoglobin of *Lumbricus terrestris. Proc. Natl. Acad. Sci. USA.* 83:8034–8038.

Vinogradov, S. N., P. K. Sharma, A. N. Qabar, J. S. Wall, J. A. Westrick, J. H. Simmons, and S. J. Gill. 1991. A dodecamer of globin chains is the principal functionnal subunit of the extracellular hemoglobin of *Lumbricus terrestris. J. Biol. Chem.* 266:13091–13096.

Ward, J. H., Jr. 1963. Hierarchical grouping to optimize an objective function. *J. Am. Statist. Assoc.* 58:236–244.

Weber, R. E., H. Malte, H. Braswell, R. W. A. Oliver, B. N. Green, P. K. Sharma, A. Kuchumov, and S. N. Vinogradov. 1995. Mass spectrometric composition, molecular mass and oxygen binding of *Macrobdella decora* hemoglobin and its tetramer and monomer subunits. *J. Mol. Biol.* 251:703–720.